Manuscript (contains title page) Click here to view linked References

Short Communication

Submission to: ANM

Title: A comparison of five partial volume correction methods for Tau and Amyloid PET imaging with [^{18}F]THK5351 and [^{11}C]PIB

Short running title: 5 partial volume corrections for tau and amyloid PET imaging

Authors: (14)

Miho Shidahara[1, 2], Benjamin A. Thomas[3,4], Nobuyuki Okamura[5], Masanobu Ibaraki[6], Keisuke Matsubara[6], Senri Oyama[1], Yoichi Ishikawa[7], Shoichi Watanuki[2], Ren Iwata[7], Shozo Furumoto[7], Manabu Tashiro[2], Kazuhiko Yanai[8], Kohsuke Gonda[1] and Hiroshi Watabe[9]

1. Department of Medical Physics, Tohoku University Graduate School of Medicine, Sendai, JAPAN.
2. Division of Cyclotron, Nuclear Medicine, Cyclotron and Radioisotope Center, Tohoku University, Sendai, JAPAN.
3. A*STAR-NUS Clinical Imaging Research Centre, Singapore, Singapore.
4. Institute of Nuclear Medicine, University College London, London, UK.
5. Division of Pharmacology, Faculty of Medicine, Tohoku Medical and Pharmaceutical University, Sendai, JAPAN.
6. Department of Radiology and Nuclear Medicine, Research Institute for Brain and Blood Vessels-Akita, Akita, JAPAN.
7. Division of Radiopharmaceutical Chemistry, Cyclotron and Radioisotope Center, Tohoku University, Sendai, JAPAN.
8. Department of Pharmacology, Tohoku University School of Medicine, Sendai, JAPAN.
9. Division of Radiation Protection and Safety Control, Cyclotron and Radioisotope Center, Tohoku University, Sendai, JAPAN.

Correspondence to:

Miho Shidahara (shidahara@med.tohoku.ac.jp), Department of Medical Physics, Tohoku University Graduate School of Medicine, Sendai, JAPAN.

Word count of the manuscript:

3189 / 3000 words

Abstract

Purpose: To suppress partial volume effect in brain PET, there has been many algorithms proposed. However, each methodology has different property due to its assumption and algorithms. Our aim of this study was to investigate the difference among PVC method for tau and amyloid PET study.

Method: We investigated two of the most commonly used partial volume correction (PVC) methods, Müller-Gärtner (MG) and geometric transfer matrix (GTM) and also other three methods for clinical tau and amyloid PET imaging. One healthy control (HC) and one Alzheimer's disease (AD) PET studies of both [^{18}F]THK5351 and [^{11}C]PIB were performed using a Eminence STARGATE scanner (Shimadzu Inc., Kyoto, Japan). All PET images were corrected for partial volume effect (PVE) by MG, GTM, Labbé (LABBE), Regional voxel-based (RBV), and Iterative Yang (IY) methods, with segmented or parcellated anatomical information processed by FreeSurfer, derived from individual MR images. PVC results of 5 algorithms were compared with the uncorrected data.

Results: In regions of high uptake of [^{18}F]THK5351 and [^{11}C]PIB, different PVCs demonstrated different SUVRs. The degree of difference between PVE uncorrected and corrected depends on not only PVC algorithm but also type of tracer and subject condition.

Conclusion: Presented PVC methods are straight-forward to implement but the corrected images require careful interpretation as different methods result in different levels of recovery.

Key words: Partial volume correction, tau PET, image processing, [^{18}F]THK5351

Introduction

In vivo brain imaging of neurofibrillary tangle (tau) and amyloid β peptide (amyloid) using Positron Emission Tomography (PET) has been recognized as having an important role in the diagnosis of early Alzheimer's disease (AD) (1). However, the PET image always suffers from partial volume effect (PVE) due to the spatial resolution of PET system, where regional uptake of radiotracer is blurred and its quantification is degraded (2).

To compensate PVE on PET images, there have been many partial volume correction (PVC) methods proposed. For brain PET studies, both the spatial resolution and individual structural images have been utilized for PVC. This is particularly relevant with the development of PET/MRI scanner (3, 4). The classical and popular PVC methods for brain PET which utilize structural information, are Müller-Gärtner (MG) (5) and the geometric transfer matrix (GTM) methods (6). MG is a voxel-based method and assumes that uptake in white matter can be accurately represented by its mean value. GTM is a region-of-interest (ROI) based method and assumes a uniform distribution within each ROIs.

There have been several reports which state that applying PVC improved image quality of tau and amyloid PET and improved the accuracy and precision of the quantification of tracer uptake (7-16). However, in many cases, the applied PVC method were limited to MG or GTM. Furthermore, Greve et al. reported that different PVC methods (MG, GTM, and Meltzer) result in different conclusions in a FDG cross-sectional aging study of elderly subjects (17). There is a need to perform a comparison study of the popular PVC methods for tau and amyloid PET studies and to explore the possibility of other PVC techniques. In this study, we report 5 methods for tau and amyloid PET images: traditional MG, GTM, and other 3 methods. The methodology was applied to PET images of a single HC and AD subjects having both [^{18}F]THK5351 and [^{11}C]PIB studies.

Material and Methods

Clinical studies

PET and MR images of 1 HC (81 y.o., Female) and 1 AD (80 y.o., Male) subjects, who had both a [^{11}C]PIB and [^{18}F]THK5351 PET scan, were used in this study. The PET studies were performed using Eminence STARGATE (Shimadzu Inc., Kyoto, Japan) with 3.5-mm (transaxial) and 5.0 mm (axial) full width at half maximum (FWHM) resolution at 1.0 cm off-center of the field of view. After a 10-min ^{131}Cs transmission scan, 60- and 70-min dynamic scanning was started immediately after the intravenous administration of 304.9-347.4 MBq [^{11}C]PIB and 176.1-178.0 MBq [^{18}F]THK5351, respectively. All emission data were reconstructed using 3D-DRAMA

(1 iteration, 128 filter cycle, 30 relaxation factor) (18) with attenuation and scatter corrections (19) and post filter of three dimensional Gaussian (3 mm FWHM). SUV images with 40-60 min time frame images were obtained. All subjects underwent T1-weighted magnetic resonance imaging (MRI) scans using a Signa 1.5-T machine (General Electric Inc., Milwaukee, WI, USA). Image matrix of reconstructed PET and MRI were 128 × 128 × 79 (2.0 × 2.0 × 2.6 mm) and 256 × 256 × 124 (0.98 × 0.98 × 1.4 mm), respectively.

This study was approved by the Ethics Committee on Clinical Investigations of Tohoku University School of Medicine and was performed in accordance with the Declaration of Helsinki. Written informed consent was obtained from all subjects after a complete description of the study had been provided.

Partial Volume Correction methods

5 PVC methods, MG (5), GTM (6, 20), Labbé (LABBE) (21), Regional voxel-based (RBV) (22), and Iterative Yang (IY) (3), were performed in this study and are described briefly below. Abbreviations are defined in **Table. 1**.

The MG (5) is voxel-based method for gray matter regions with the assumption of uniform-tracer uptake in white matter. Basic concept of MG is that uncorrected PET image, $f(x)$, can be decomposed into gray matter and white matter (CSF if necessary) components. PVE corrected PET image of gray matter region, $f_{c,gray}(x)$, is estimated by the subtraction from $f(x)$ to smoothed PET image of white matter region and then divided by gray matter fractions in each pixel, as follows.

$$f_{c,gray}(x) = \frac{f(x) - A_{white,f(x)} \cdot p_{white}(x) \otimes PSF}{p_{gray}(x) \otimes PSF} . \quad (1)$$

The GTM method (6, 20) is ROI-based method. GTM also utilizes the assumption that PET image can be decomposed into regions where can be regarded as the uniform activity within it. Averaged values of $f(x)$ in the i-th region, $A_{i,f(x)}$, is multiplied with inverse-matrix of **T** (**A** = **T** · **C**) and then corrected values, $C_{i,f(x)}$, for every region are obtained as follows,

$$\begin{bmatrix} C_{1,f(x)} \\ \vdots \\ C_{i,f(x)} \\ \vdots \\ C_{N,f(x)} \end{bmatrix} = \mathbf{T}^{-1} \begin{bmatrix} A_{1,f(x)} \\ \vdots \\ A_{i,f(x)} \\ \vdots \\ A_{N,f(x)} \end{bmatrix}, \quad (2)$$

where **T** is the geometric transfer matrix of t_{ij}, which represents the contribution of spill-over from D_i into D_j.

The LABBE (21) is also a ROI-based method. LABBE also utilizes the assumption that PET image can be decomposed into regions where can be regarded as the uniform activity within it. Sets of PET value at each voxel,[$f(x_1)$, $f(x_2)$, ….., $f(x_M)$], is multiplied with inverse-matrix of **T** (**f** = **T** · **C**) and then corrected values, $C_{i,f(x)}$, for every region are obtained as follows,

$$\begin{bmatrix} C_{1,f(x)} \\ \vdots \\ C_{i,f(x)} \\ \vdots \\ C_{N,f(x)} \end{bmatrix} = \mathbf{T}^{-1} \begin{bmatrix} f(x_1) \\ \vdots \\ f(x_j) \\ \vdots \\ f(x_M) \end{bmatrix}, \tag{3}$$

Where **T** is the matrix calculated by $PSF \otimes p_i(x)$ and M is the total pixel number.

The RBV (22) is an extension of the GTM and the voxel-wise correction of Yang et al.(23). Basic concept of RBV is to multiply uncorrected PET image $f(x)$ with PVE correction factor in each voxel. The factor is derived from the ratio between synthetic PET image, consists of PVE corrected ROI values by GTM, and smoothed synthetic PET image as follows;

$$\begin{aligned} f_c(x) &= f(x) \cdot \left[\frac{f_s(x)}{f_s(x) \otimes PSF} \right] \\ f_s(x) &= \sum_{i=1}^{N} \left[C_{i,f(x)} \cdot p_i(x) \right] \end{aligned} \quad . \tag{4}$$

The Iterative Yang (IY) (3) is similar with RBV but a further adaptation of the Yang method (23). This process is iterated several times with iteration number k (where iteration number was set to 5 in this study). PVE correction factor for IY is derived from the ratio between synthetic PET image, consists of ROI value of k-th corrected $f_c^k(x)$ and smoothed synthetic PET image as follows,

$$\begin{aligned} f_c^0(x) &= f(x) \\ f_c^{k+1}(x) &= f(x) \cdot \left[\frac{f_s^k(x)}{f_s^k(x) \otimes PSF} \right] \\ f_s^k(x) &= \sum_{i=1}^{N} \left[A_{i,f_c^k(x)} \cdot p_i(x) \right] \end{aligned} \quad . \tag{5}$$

Data Processing and Analysis

The subject MR image was parcellated using the FreeSurfer software package (surfer.nmr.mgh.harvard.edu) version 5.1 (24-27). FreeSurfer extracts cortical surface meshes from the structural MR and assigns anatomical labels based on probabilistic data derived from a manually labeled training set. All processing using FreeSurfer was performed without any manual intervention by the user, except for the hippocampus of the AD subject. The hippocampi of the AD subject was manually re-drawn and carefully checked by a physician because FreeSurfer overestimated volume of atrophied thin hippocampi by including enlarged ventricles. The detailed parcellation produced by FreeSurfer was then mapped into 50 regions. The assignment of these regions is shown in **supplementary table 1**.

PVC images after MG, GTM, LABBE, RBV, and IY correction were implemented using the PETPVC toolbox (https://github.com/UCL/PETPVC) (28) and were applied assuming a resolution of 5 mm FWHM. 10 iterations were performed for IY. Both uncorrected and PVC images with [^{18}F]THK5351 and [^{11}C]PIB were normalized with averaged ROI value in cerebellar grey matter to generate SUVR images. Through ROI analysis, we evaluated the effect of the different 5 PVC algorithms.

Results

Figure 1 and **2** shows the uncorrected and 2 voxel-based PVC SUVR images of 1 AD and 1 HC with [^{18}F]THK5351 and [^{11}C]PIB, respectively. After PVCs of the AD subject by RBV and MG, hippocampal SUVR of [^{18}F]THK5351 (**Figure 1** upper) and cortical the SUVR of [^{11}C]PIB (**Figure 2** upper) were visually increased compared with the uncorrected. **Figure 3** shows SUVR values of uncorrected PET images, 3 voxel-based and 2 ROI-based PVC results of the HC and AD subjects, for both tracers. **Figure 4** also shows %difference of SUVR for 5 PVCs against the uncorrected. For AD subject, the amount of recovery by RBV and IY were almost the same, similar with that of GTM, but different from those of MG and LABBE (e.g. hippocampus of AD in [^{18}F]THK5351 and frontal of AD in [^{11}C]PIB) (**Figure 4A** and **4B**). For HC subject, MG showed small increase of tracer uptake compared with other 4 methods (**Figure 4C** and **4D**).

Discussion

In the present study, we compared five partial volume correction methods for tau and amyloid PET imaging. Subjects undergoing tau and amyloid PET imaging are often expected to have brain atrophy, with or without physiological change in the region. It is difficult to accurately quantify tracer uptake in atrophic regions due to PVE. PVC for tau and amyloid PET imaging is expected to compensate PVE for more accurate quantification of tracer uptake, and is therefore essential

for these applications (10).

However, the present results suggest that most PVC techniques can produce different amounts of recovery in each region, subject condition, and tracer, even though RBV and IY showed the same results. In particular, MG showed different amount of recovery between subject conditions. Thomas et al previously investigated the quantification of PVCs (RBV, MG, modified MG, deconvolution approach Van-Cittered) on [^{11}C]PIB human mimicked brain Phantom with two conditions, HC and AD (22). Notably, after PVC of MG, overestimation of [^{11}C]PIB uptake in the hippocampal region of an AD phantom was observed, even though that of a HC phantom was not (22). We also observed a similar tendency with this correction technique. This indicates that tracer uptake in the hippocampal region after MG PVC may lead to a misinterpretation of pathological change.

Limitation of the study is only two subjects involved, therefore, it is difficult to conclude directionality of what PVC would be better. In this paper, we showed the potential that different PVC may cause different quantitative values and distributions. PVC is sensitive to errors in image processing, for example of mis-segmentation of, and mis-co-registration to, an anatomical image, and appropriate setting of the estimated PSF for corrections. Not only algorithms but also these sources of error propagation need to be considered carefully to increase potential usage of PV-corrected PET images. These are out of scope of this report but in order to compare and optimize the algorithm of PVC, further simulation and clinical studies with sufficient number of the subject would be necessary and this will be our future work.

Conclusion

PVC is essential processing when studying populations that are likely to have atrophy. However, in regions of high uptake of [^{18}F]THK5351 and [^{11}C]PIB, different PVCs demonstrated different SUVRs. The degree of difference between PVE uncorrected and corrected data depends on not only PVC algorithm but also subject/patient disease. Presented PVC methods are straight-forward to implement but careful interpretation of the results is necessary.

Figure and Table legends

Figure 1. Uncorrected and two PVC SUVR images for single HC and AD subject with [^{18}F]THK5351

Figure 2. Uncorrected and 2 PVC SUVR images for single HC and AD subject with [^{11}C]PIB

Figure 3. ROI comparison of uncorrected and PVC SUVRs for a HC and AD subject with [^{18}F]THK5351 and [^{11}C]PIB.

Figure 4. %Difference between uncorrected and PVC SUVRs for a HC and AD subject with [^{18}F]THK5351 and [^{11}C]PIB.

Table 1. Definitions and abbreviations for PVC processing

References

1. Okamura N, Harada R, Furukawa K, Furumoto S, Tago T, Yanai K, et al. Advances in the development of tau PET radiotracers and their clinical applications. Ageing research reviews. 2016.

2. Soret M, Bacharach SL, Buvat I. Partial-volume effect in PET tumor imaging. J Nucl Med. 2007;48(6):932-45.

3. Erlandsson K, Buvat I, Pretorius PH, Thomas BA, Hutton BF. A review of partial volume correction techniques for emission tomography and their applications in neurology, cardiology and oncology. Physics in medicine and biology. 2012;57(21):R119-59.

4. Erlandsson K, Dickson J, Arridge S, Atkinson D, Ourselin S, Hutton BF. MR Imaging-Guided Partial Volume Correction of PET Data in PET/MR Imaging. PET clinics. 2016;11(2):161-77.

5. Muller-Gartner HW, Links JM, Prince JL, Bryan RN, McVeigh E, Leal JP, et al. Measurement of radiotracer concentration in brain gray matter using positron emission tomography: MRI-based correction for partial volume effects. Journal of cerebral blood flow and metabolism : official journal of the International Society of Cerebral Blood Flow and Metabolism. 1992;12(4):571-83.

6. Rousset OG, Ma Y, Evans AC. Correction for partial volume effects in PET: principle and validation. Journal of nuclear medicine 1998;39(5):904-11.

7. Adamczuk K, De Weer AS, Nelissen N, Chen K, Sleegers K, Bettens K, et al. Polymorphism of brain derived neurotrophic factor influences beta amyloid load in cognitively intact apolipoprotein E epsilon4 carriers. NeuroImage Clinical. 2013;2:512-20.

8. Brendel M, Hogenauer M, Delker A, Sauerbeck J, Bartenstein P, Seibyl J, et al. Improved longitudinal [(18)F]-AV45 amyloid PET by white matter reference and VOI-based partial volume effect correction. NeuroImage. 2015;108:450-9.

9. Forster S, Yousefi BH, Wester HJ, Klupp E, Rominger A, Forstl H, et al. Quantitative longitudinal interrelationships between brain metabolism and amyloid deposition during a 2-year follow-up in patients with early Alzheimer's disease. European journal of nuclear medicine and molecular imaging. 2012;39(12):1927-36.

10. Ito H, Shinotoh H, Shimada H, Miyoshi M, Yanai K, Okamura N, et al. Imaging of amyloid deposition in human brain using positron emission tomography and [18F]FACT: comparison with [11C]PIB. European journal of nuclear medicine and molecular imaging. 2014;41(4):745-54.

11. Matsubara K, Ibaraki M, Shimada H, Ikoma Y, Suhara T, Kinoshita T, et al. Impact of spillover from white matter by partial volume effect on quantification of amyloid deposition with [11C]PiB PET. NeuroImage. 2016;143:316-24.

12. Mori T, Shimada H, Shinotoh H, Hirano S, Eguchi Y, Yamada M, et al. Apathy correlates with prefrontal amyloid beta deposition in Alzheimer's disease. Journal of neurology, neurosurgery, and psychiatry. 2014;85(4):449-55.
13. Rullmann M, Dukart J, Hoffmann KT, Luthardt J, Tiepolt S, Patt M, et al. Partial-Volume Effect Correction Improves Quantitative Analysis of 18F-Florbetaben beta-Amyloid PET Scans. J Nucl Med. 2016;57(2):198-203.
14. Scholl M, Lockhart SN, Schonhaut DR, O'Neil JP, Janabi M, Ossenkoppele R, et al. PET Imaging of Tau Deposition in the Aging Human Brain. Neuron. 2016;89(5):971-82.
15. Su Y, Blazey TM, Snyder AZ, Raichle ME, Marcus DS, Ances BM, et al. Partial volume correction in quantitative amyloid imaging. NeuroImage. 2015;107:55-64.
16. Villemagne VL, Furumoto S, Fodero-Tavoletti MT, Mulligan RS, Hodges J, Harada R, et al. In vivo evaluation of a novel tau imaging tracer for Alzheimer's disease. European journal of nuclear medicine and molecular imaging. 2014;41(5):816-26.
17. Greve DN, Salat DH, Bowen SL, Izquierdo-Garcia D, Schultz AP, Catana C, et al. Different partial volume correction methods lead to different conclusions: An F-FDG-PET study of aging. NeuroImage. 2016;132:334-43.
18. Tanaka E, Kudo H. Optimal relaxation parameters of DRAMA (dynamic RAMLA) aiming at one-pass image reconstruction for 3D-PET. Physics in medicine and biology. 2010;55(10):2917-39.
19. Ibaraki M, Matsubara K, Sato K, Mizuta T, Kinoshita T. Validation of a simplified scatter correction method for 3D brain PET with 15O. Annals of nuclear medicine. 2016;30(10):690-8.
20. Rousset OG, Collins DL, Rahmim A, Wong DF. Design and implementation of an automated partial volume correction in PET: application to dopamine receptor quantification in the normal human striatum. Journal of nuclear medicine : official publication, Society of Nuclear Medicine. 2008;49(7):1097-106.
21. Labbe C, Koepp MJ, Ashburner J, Spinks T, Richardson M, Duncan JS, et al. Absolute PET quantification with correction for partial volume effects within cerebral structures. Carson RE, Daube-Witherspoon ME, Herscovitch P, editors: Academic Press; 1998.
22. Thomas BA, Erlandsson K, Modat M, Thurfjell L, Vandenberghe R, Ourselin S, et al. The importance of appropriate partial volume correction for PET quantification in Alzheimer's disease. European journal of nuclear medicine and molecular imaging. 2011;38(6):1104-19.
23. Yang C, Huanf C, Mega M, Lin KP, Toga AW, Small GW, et al. Investigation of Partial Volume Correction Methods for Brain FDG PET Studies. IEEE Trans Nucl Sci. 1996;43(6):3322-7.

24. Dale AM, Fischl B, Sereno MI. Cortical surface-based analysis. I. Segmentation and surface reconstruction. NeuroImage. 1999;9(2):179-94.

25. Fischl B, Dale AM. Measuring the thickness of the human cerebral cortex from magnetic resonance images. Proceedings of the National Academy of Sciences of the United States of America. 2000;97(20):11050-5.

26. Fischl B, Sereno MI, Dale AM. Cortical surface-based analysis. II: Inflation, flattening, and a surface-based coordinate system. NeuroImage. 1999;9(2):195-207.

27. Segonne F, Pacheco J, Fischl B. Geometrically accurate topology-correction of cortical surfaces using nonseparating loops. IEEE transactions on medical imaging. 2007;26(4):518-29.

28. Thomas BA, Cuplov V, Bousse A, Mendes A, Thielemans K, Hutton BF, et al. PETPVC: a toolbox for performing partial volume correction techniques in positron emission tomography. Physics in medicine and biology. 2016;61(22):7975-93.

Table 1. Definitions and abbreviations for PVC processing

Abbreviation	Description
$f(x)$	uncorrected PET image
$f_c(x)$	PVE corrected PET image
$f_s(x)$	synthetic PET image
$p_i(x)$	anatomical probability of i-th region at location x
N	the total number of regions
$A_{i,f(x)}$	Averaged value of $f(x)$ at i-th region
$C_{i,f(x)}$	PVE corrected value for $f(x)$ at i-th region
D_i	Volume of i-th region
PSF	Point spread function
$\otimes$	Operation of three-dimensional convolution integral.

Figure

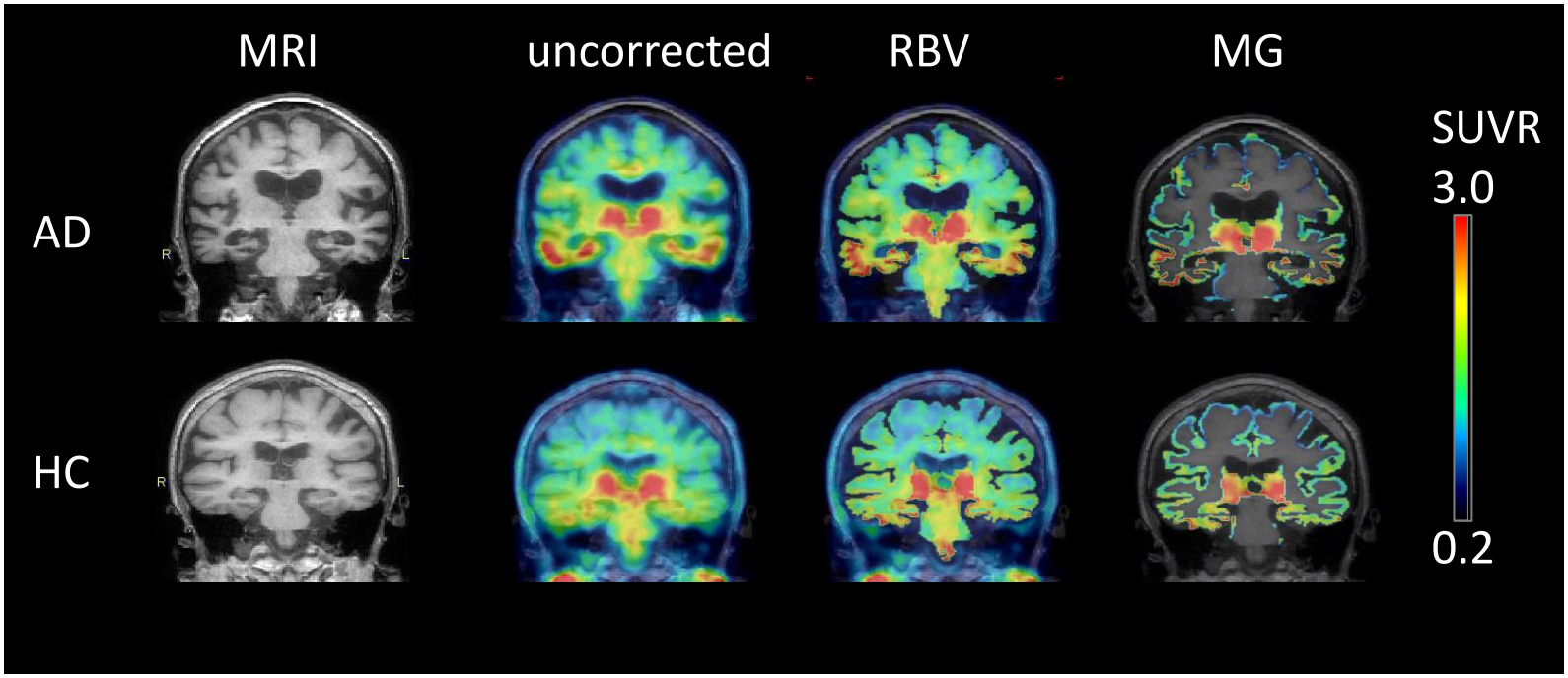

Figure 1. Uncorrected and 2 PVC SUVR images for single HC and AD subject with [^{18}F]THK5351

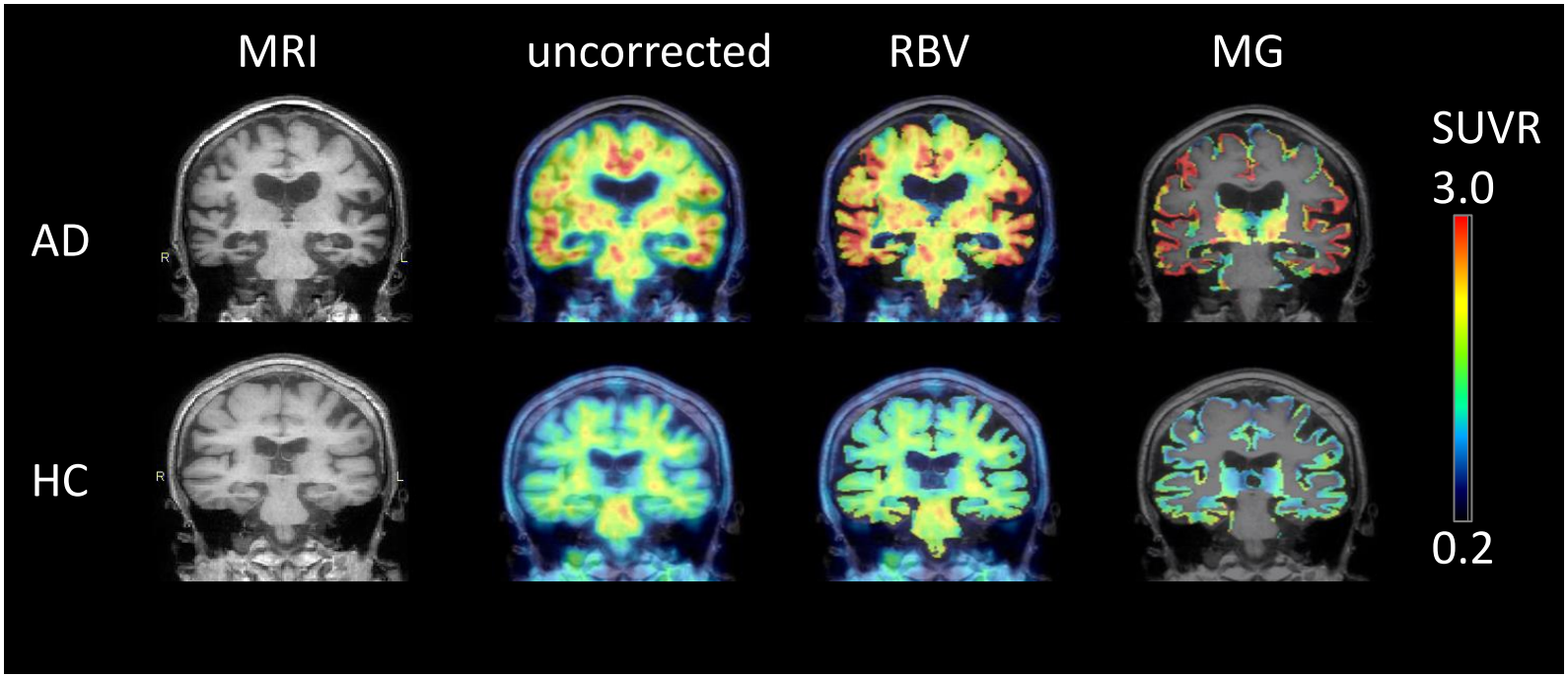

Figure 2. Fig. 2 Uncorrected and 2 PVC SUVR images for single HC and AD subject with [^{11}C]PIB

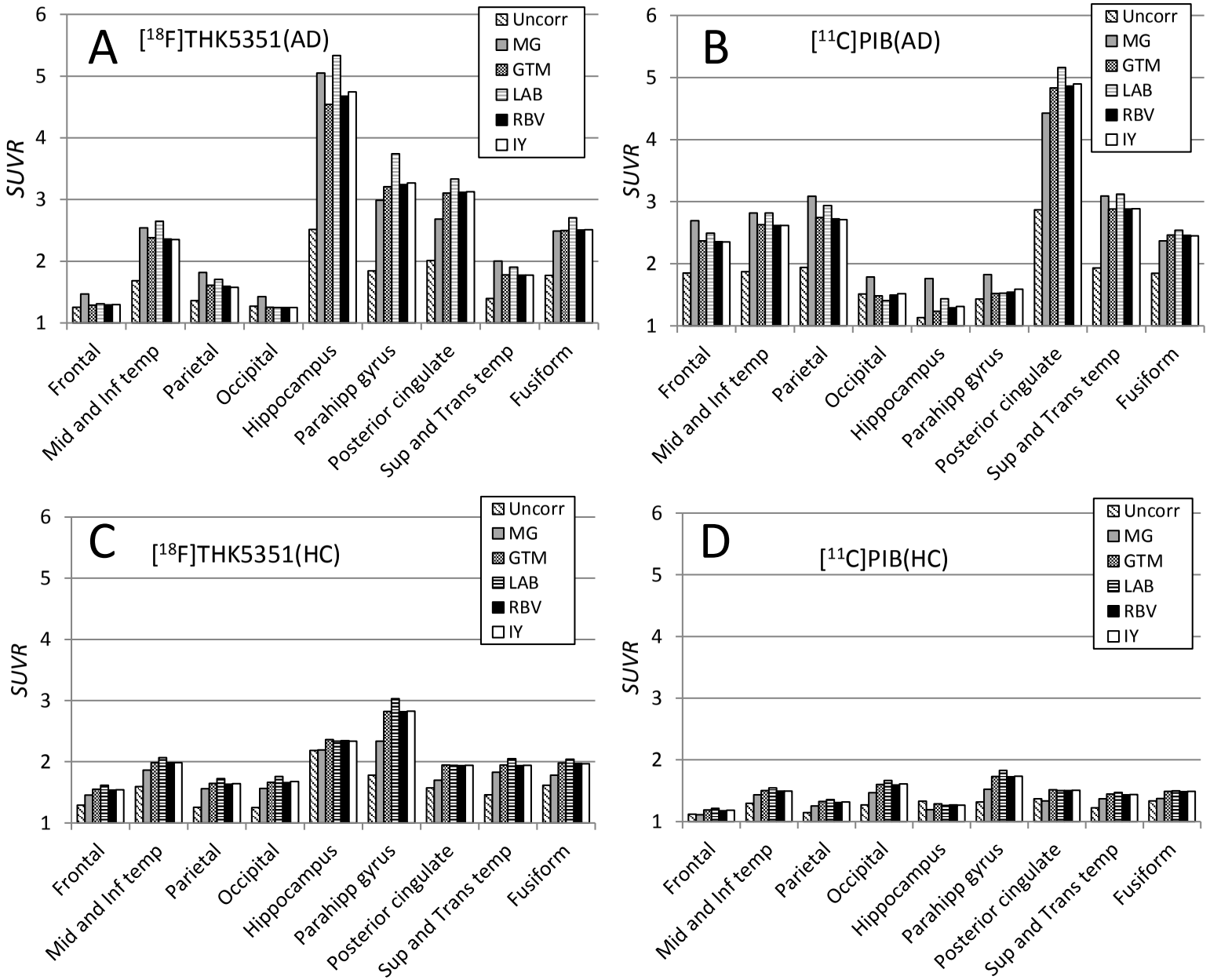

Figure 3. ROI comparison of uncorrected and PVC SUVRs for a HC and AD subject with [18F]THK5351 and [11C]PIB.

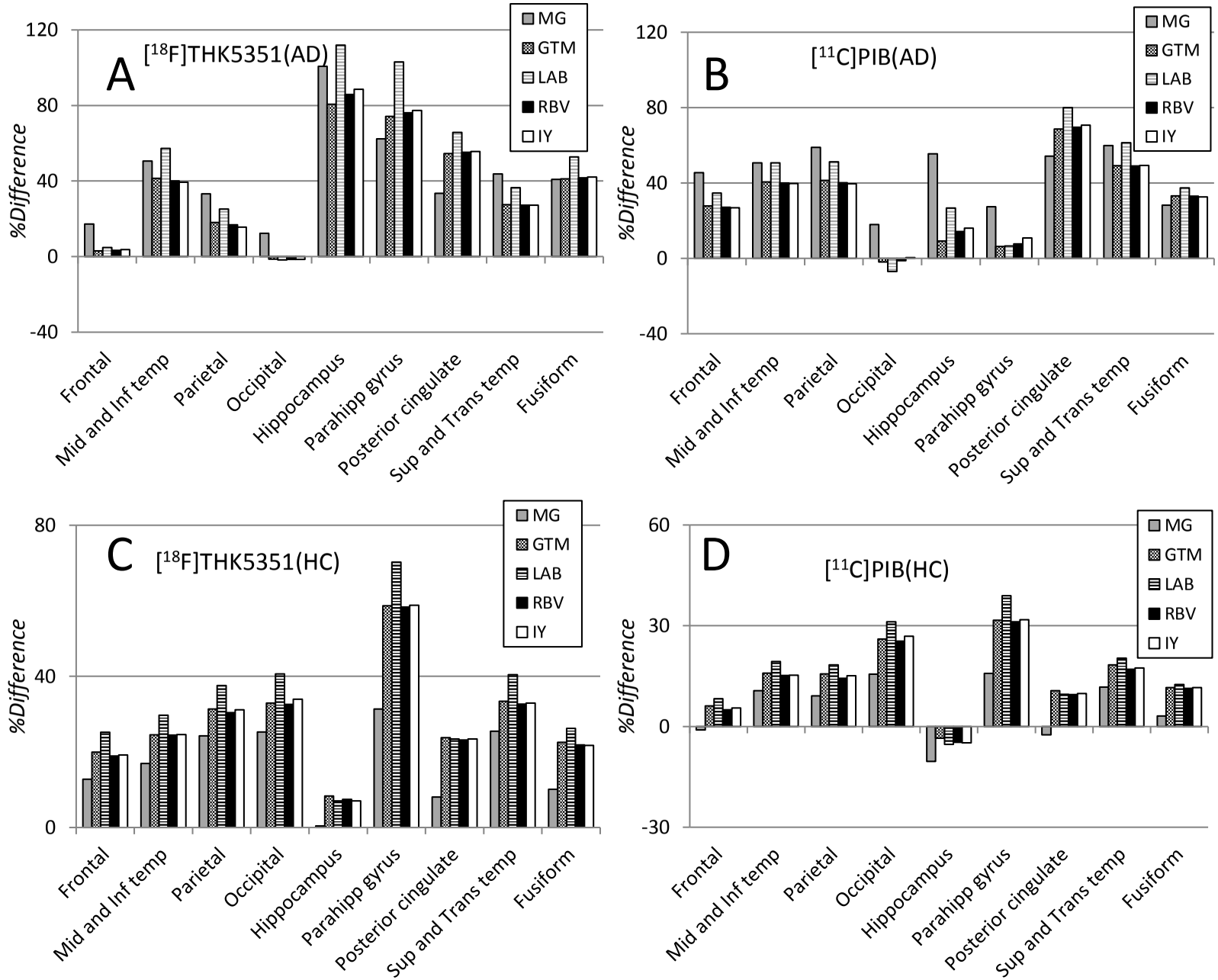

Figure 4. %Difference between uncorrected and PVC SUVRs for a HC and AD subject with [^{18}F]THK5351 and [^{11}C]PIB.